THAI NGUYEN UNIVERSITY
UNIVERSITY OF EDUCATION

NGUYEN THI THUY HANG

SYNTHESIS AND INVESTIGATION OF THE RHODAMINE B DEGRADATION CAPABILITY OF NANO FERRITE MATERIALS IN AQUEOUS ENVIRONMENT

Speciality: Inorganic chemistry
Code: 9440113

DISSERTATION SUMMARY

THAI NGUYEN - 2023

The dissertation was finished at:

UNIVERSITY OF EDUCATION - THAI NGUYEN UNIVERSITY

Supervisors:

1. Assoc. Prof. Dr. Le Huu Thieng.
2. Assoc. Prof. Dr. Nguyen Thi To Loan.

Reviewer 1:……

Reviewer 2:……

Reviewer 3:…….

The dissertation will be defended in the university committee:

UNIVERSITY OF EDUCATION - THAI NGUYEN UNIVERSITY

At ……....., 2023

The dissertation can be read at:

- National library of Vietnam;
- Digital Center - Thai Nguyen University;
- Library of University of Education.

INTRODUCTION

Nowadays, the development of industries causes the pollution of the environment, especially the water environment, which is polluted with persistent organic compounds and heavy metals, leading to severe diseases in humans and negative impacts on the environment. The photocatalytic method is an effective treatment method for decomposing organic compounds in the water environment. This method is based on using semiconductors and light sources for the degradation of organic substances. The outstanding features of the photocatalytic method are environmental friendliness and the capability of completely decomposing organic pollutants into non-toxic inorganic substances such as CO_2 and H_2O.

Nanomaterials have been widely studied and applied in many fields due to their diversity of structural composition, ease of forming solid solutions, and unique physical and chemical properties such as hardness and corrosion resistance. Spinel ferrite materials are used as information storage materials, sensors, optoelectronic recording materials, photocatalysts, etc. The properties of these materials depend on the synthesis method and conditions that determine the crystallinity, purity, particle shape and size of the materials.

Spinel ferrites, with the general formula MFe_2O_4 (M = Mn, Fe, Co, Ni, Zn...), are one of the most promising photocatalytic materials due to their ability to absorb visible light and can be easily separated from the system owing to their magnetic property, leading to the effectively reduced costs and high practical applicability.

The advantage of the ferrite spinel catalytic system is the simultaneous occurrence of heterogeneous Photon and Fenton processes in the presence of H_2O_2 and visible light, helping the decomposition of organic compounds to be highly effective. The photocatalytic activity of pure ferrite systems has been studied by many scientists. The performance of the photocatalytic reaction in the presence of ferrite depends on several factors, such as morphology, particle size, and substituted metal ions in the ferrite network... Many studies show that when doped II or III valence

metal ions, the structure, morphology, and photocatalytic performance of ferrites change.

When rare earth ions such as La^{3+}, Nd^{3+}, Eu^{3+}, and Gd^{3+} are doped into ferrite, they can replace Fe^{3+} ions at octahedral sites within the crystal lattice, causing the crystal lattice to deform and resulting in an increase or decrease in the lattice constant.

However, nano ferrite materials exhibit strong interparticle interactions, leading to agglomeration and challenging their recovery after large-scale processing. One way to address this drawback is to disperse the ferrite nanoparticles onto a suitable carrier material.

Thus, we have chosen the thesis topic: "*Synthesis and Investigation of the Rhodamine B Degradation Capability of Nano Ferrite Materials in Aqueous Environment.*"

Thesis Objective:

This thesis aims to synthesize a variety of spinel ferrite systems with high catalytic activity for the treatment of organic pollutants in water environments.

Research Content:

The effects of some factors of the synthesis process on the phase composition, morphology, and properties of ferrite materials MFe_2O_4 (M =Zn, Co, Ni) have been studied.

Pure ferrite materials ($ZnFe_2O_4$, $CoFe_2O_4$, and $NiFe_2O_4$), ferrite materials doped rare earth ions (La^{3+}, Nd^{3+}), and $ZnFe_2O_4$/Bentonite composite material have been synthesized. Their characteristics, properties, and rhodamine B photocatalytic degradation activity have been investigated.

The ability of ferrite-containing materials to recover, reuse, and treat textile wastewater has been evaluated.

New Aspects of the Thesis

The effect of factors, including calcination temperature, calcination time, and metal ion/urea molar ratio, on the phase formation, morphology, and properties of ferrite materials ($ZnFe_2O_4$, $CoFe_2O_4$, and $NiFe_2O_4$) has been determined. Among those factors, calcination temperature and

metal/urea molar ratio are two factors that strongly affect the RhB photocatalytic degradation activity of $CoFe_2O_4$ and $NiFe_2O_4$.

Ferrite systems ($ZnFe_2O_4$, $CoFe_2O_4$) doped with rare earth ions La^{3+} and Nd^{3+} have been successfully synthesized. Their structural characteristics, properties, and rhodamine B photocatalytic degradation activity have been systematically investigated.

$ZnFe_2O_4$/Bentonite composite material has been successfully synthesized. Its structural characteristics, properties, and rhodamine B photocatalytic degradation activity have been examined. When the composite system forms, the agglomeration of ferrite particles is reduced, the specific surface area of the material increases, and the photocatalytic performance is improved.

The synthesized ferrite-containing materials are relatively stable, have high reuse efficiency, and can be applied to treat organic pollutants in textile and dyeing villages.

CHAPTER 1: LITERATURE REVIEW

1.1. Introduction to Spinel Ferrite

1.1.1. General Structure of Spinel Ferrite

Spinel is a group of compounds with a general formula AB_2O_4 (where A represents divalent cations, and B represents trivalent cations). Divalent cations can include Cu^{2+}, Be^{2+}, Mg^{2+}, Ca^{2+}, Sr^{2+}, Ba^{2+}, Zn^{2+}, Mn^{2+}, Fe^{2+}, Co^{2+}, Ni^{2+}… Trivalent cations consist of Al^{3+}, Cr^{3+} , Fe^{3+}, and less commonly Ga^{3+}, In^{3+}, La^{3+}, Ti^{3+}, V^{3+}, Sb^{3+}…The crystal structure of spinel is illustrated in Figure 1.1.

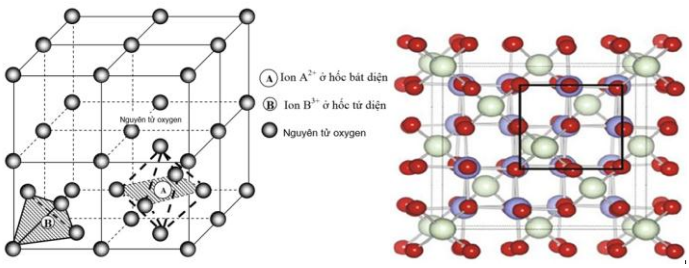

Figure 1.1. Crystal Structure Model of Spinel

To synthesize the spinel ferrite materials, we used the solution combustion method with urea as a fuel. We dissolved 0.075 moles (4.545 g) of urea in 150 mL of distilled water and then added 0.01 moles (2.615 g) of $Zn(NO_3)_2.4H_2O$ and 0.02 moles (8.080 g) of $Fe(NO_3)_3.\ 9H_2O$ to the solution. The mixture was stirred at 70°C. The sample was then dried at

70°C and calcined at 500°C for 3 hours, resulting in the $ZnFe_2O_4$ sample (Figure 2.1). It is assumed that the reactions occurred as follows:

$3Zn(NO_3)_2 + 6Fe(NO_3)_3 + 20(NH_2)_2CO \rightarrow 3ZnFe_2O_4 + 20CO_2 + 32N_2 + 40H_2O$

The $CoFe_2O_4$ and $NiFe_2O_4$ samples were synthesized using a similar procedure to the $ZnFe_2O_4$ sample. We synthesized the $ZnFe_2O_4$, $CoFe_2O_4$, and $NiFe_2O_4$ samples following the same synthesis process as mentioned earlier, with variations in certain parameters such as calcination temperature (from 500 to 800°C), calcination time (from 1 to 4 hours), metal-to-urea molar ratio (from 3/1 to 1/3), and pH (from 1 to 5).

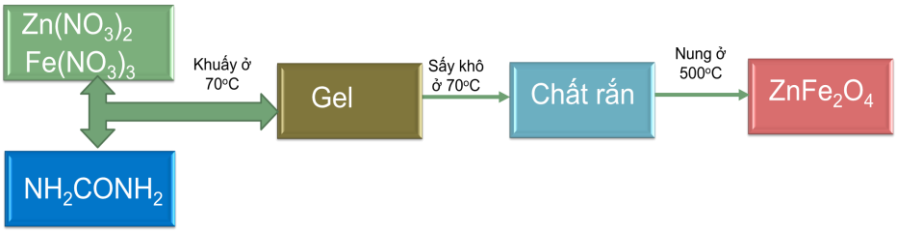

Figure 2.1. Schematic of Spinel Ferrite Synthesis by Solution Combustion Method

2.3.2. Synthesis of Ferrite Materials doped with Rare Earth Ions

The ferrite materials doped with rare earth ions (La^{3+}, Nd^{3+}) were synthesized similarly to the pure ferrite samples, with the addition of $La(NO_3)_3$ or $Nd(NO_3)_3$ salts in appropriate molar ratios (as shown in Tables 2.3-2.5). The schematic of the synthesis process is illustrated in Figure 2.2. It is assumed that the synthesis reactions occurred as follows:

$3Zn(NO_3)_2 + 3(2-x)Fe(NO_3)_3 + 3xLa(NO_3)_3 + 20(NH_2)_2CO \rightarrow 3ZnFe_{2-x}La_xO_4 + 20CO_2 + 32N_2 + 40H_2O$

$3M(NO_3)_2 + 3(2-x)Fe(NO_3)_3 + 3xNd(NO_3)_3 + 20(NH_2)_2CO \rightarrow 3MFe_{2-x}Nd_xO_4 + 20CO_2 + 32N_2 + 40H_2O$ (M =Zn, Co).

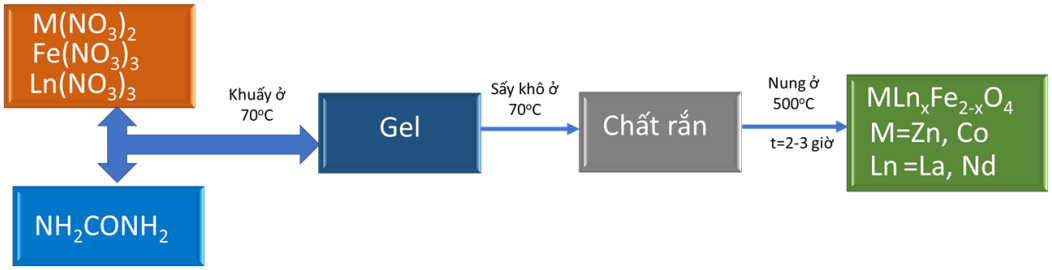

Figure 2.2. Schematic of the Synthesis of Complex Ferrite Materials MFe_2O_4 with Rare Earth Ions by the Solution Combustion Method

2.3.3. Synthesis of $ZnFe_2O_4$/Bentonite Composite Materials

Firstly, 6.64 g of urea was dissolve in 150 mL of distilled water, then 4.33 grams of $Zn(NO_3)_2.4H_2O$ and 13.41 grams of $Fe(NO_3)_3.9H_2O$ were added to obtain solution A. Bentonite was dispersed in ammonia solution under ultrasonic condition for 15 minutes (mixture B). The mixture B was mixed with solution A and magnetically stirred at 70^oC for 4 hours. The samples were dried at 70^oC, then calcined at 500^oC in 3 hours. The obtained product is $ZnFe_2O_4$/Bentonite (symbolized as $ZnFe_2O_4$/BT). Pure $ZnFe_2O_4$ and $ZnFe_2O_4$/BT samples were synthesized under the same conditions.

2.4. Investigating the photocatalytic activity of Rhodamine B decomposition of material systems

2.4.1. Preparing a calibration curve to determine Rhodamine B concentration

Firstly, rhodamine B (RhB) solutions with concentrations from 1÷10 mg/L were prepared at pH = 7 . Then, the absorbance of the above solution series was measured at a wavelength of 553 nm and the obtained equation for the callibration curve is y=0.1691x + 0.0492, where y is the absorbance, and x is the concentration.

2.4.2. Effect of reaction conditions

Presented in detail in the thesis.

2.4.3. Effect of metal ion/urea molar ratio

The influence of the metal ion/urea molar ratio (M/U) during sample synthesis on the photocatalytic activity of RhB decomposition of $NiFe_2O_4$ was investigated. We selected 3 M/U molar ratios of 1/2, 1/1 and 3/1. The amount of material in each experiment was 1.0 g/L; the concentration of H_2O_2 was 0.1M; the lighting time was 270 minutes. The procedure was similar to that described in section 2.4.2 for the system with ferrite material, H_2O_2, and illumination.

2.4.4. Effect of calcination temperature

The effect of calcination temperature during sample synthesis on the photocatalytic activity of RhB decomposition of $CoFe_2O_4$ was investigated in the range of 500 ÷ 800^oC. The amount of $CoFe_2O_4$ material in each experiment was 1.0 g/L; the amount of H_2O_2 was 0.15M, the lighting time

was 270 minutes. The procedure was similar to that described in section 2.4.2 for the system with ferrite material, H_2O_2 and illumination.

2.4.5. Effect of amount of doping ions

The effect of doping La^{3+} and Nd^{3+} ions on the photocatalytic activity of $ZnFe_2O_4$ and $CoFe_2O_4$ was carried out with doping ion amounts of 0÷5%. Samples were performed with a material amount of 1.0 g/L, a H_2O_2 amount of 0.1M for the $ZnLa_xFe_{2-x}O_4$ and $ZnNd_xFe_{2-x}O_4$ samples, and 0.15M for the $CoNd_xFe_{2-x}O4$ sample; the lighting time was 210 minutes. The procedure was similar to that described in section 2.4.2 for the system with ferrite material, H_2O_2 and illumination.

2.4.6. Effect of H_2O_2 concentration

The effect of H_2O_2 concentration on photocatalytic activity was conducted at concentrations of 0.05M; 0.1M, and 0.15M. Samples were done with a material amount of 1.0 g/L, illumination time of 270 minutes. The procedure was similar to that described in section 2.4.2 for the system with ferrite material, H_2O_2, and illumination.

2.4.7. Effect of material dose

The effect of material dose on photocatalytic activity was conducted with material dose varying from 0.5 ÷ 1.0 g/L. The concentration of H_2O_2 was selected based on the results in section 2.4.6. The illumination time of the samples was 240 minutes. The procedure was similar to that described in section 2.4.2 for the system with ferrite material, H_2O_2 and illumination.

2.4.8. Effects of inhibitors

To have a basis for proposing the RhB decomposition reaction mechanism, we have added to the system containing ferrite, H_2O_2, and LED lighting some substances that inhibit the formation of free radicals $^{\bullet}O_2^-$, $^{\bullet}OH$, positive hole (h^+). Specifically as follows: 1mL of 1 mM ascorbic acid solution (as $^{\bullet}O_2^-$ radical inhibitor), 1mL of 10 mM isopropylic alcohol (IPA) solution ($^{\bullet}OH$ radical inhibitor), and 1mL of 1 mM ethylenediaminetetraacetic acid (EDTA) solution (h^+ inhibitor). The procedure was similar to that described in section 2.4.2 for the system with ferrite material, H_2O_2, and illumination.

2.5. Study the possibility of recovering and reusing materials

The procedure was similar to that described in section 2.4.2 for the system with ferrite material, H_2O_2, and illumination. After each time, the materials were recovered using a magnet, washed with ethanol, and dried at 70^{o}C for 3 hours. Then, the materials were reused under the same conditions as the first time.

2.6. Testing textile wastewater treatment

Wastewater was collected from the wastewater tank of the sedge mat weaving village, located in Vu Ha village, An Vu commune, Quynh Phu district, Thai Binh province. The wastewater had a dark red color (Figure 2.4a). Dilute the initial wastewater 20 times to investigate the ability to decompose colorants in the presence of material samples $ZnLa_xFe_{2-x}O_4$ and $CoNd_xFe_{2-x}O_4$ (x =0 ÷ 0.05) (Figure 2.4b). The mineralization degree (COD%) of the samples was calculated according to the following formula:

$$COD\% = \frac{COD_o - COD_t}{COD_o} \cdot 100\%$$

Figure 2.4. Initial wastewater sample (a) and 20-time diluted solution (b)

CHAPTER 3: RESULTS AND DISCUSSION

3.1. MFe_2O_4 ferrite material system (M=Zn, Co, Ni)

3.1.1. Effect of some factors on phase formation and crystal size of ferrite MFe_2O_4 (M=Zn, Co, Ni)

3.1.1.1. Effect of calcination temperature

According to the thermal analysis (TA) diagram of gel prepared at molar ratio M/U = 1/2, the gelation temperature is 70^{o}C. From the results of TA, to obtain $ZnFe_2O_4$, $CoFe_2O_4$, $NiFe_2O_4$, it is necessary to calcine above 400^{o}C. We selected the calcination temperatures from 500 ÷ 800^{o}C for the following research. To obtain single-phase of $ZnFe_2O_4$, $CoFe_2O_4$

and $NiFe_2O_4$ with high crystallinity and small particle size, we chose the optimal sample calcination temperature of 500°C.

We recorded the FT-IR spectrum, specific surface area, scanning electron microscope (SEM), DRS, and magnetic spectra of the $CoFe_2O_4$ sample obtained at 500 ÷ 800°C.

Table 3.3. Values of wave number, specific surface area, band gap energy, and magnetic parameters of $CoFe_2O_4$ when heated at 500 ÷ 800°C

Mẫu	$\overline{\nu_1}$ (cm^{-1})	$\overline{\nu_2}$ (cm^{-1})	**S_{BET} ($m^2.g^{-1}$)**	**E_g (eV)**	**M_s (emu/g)**	**M_r (emu/g)**	**H_c (Oe)**
CF500	526	411	12,69	1,57	44,41	20,36	1739,45
CF600	530	409	7,55	1,66	53,86	22,88	1234,10
CF700	532	408	3,94	1,90	59,40	27,89	1234,20
CF800	522	412	1,58	2,03	61,80	27,83	762,04

3.1.1.2. Effect of calcination time

According to the results, the optimal calcination time was 2 hours for $CoFe_2O_4$ and $NiFe_2O_4$ and 3 hours for $ZnFe_2O_4$ to obtain single-phase and small-sized crystals.

3.1.1.3. Effect of metal ion/urea molar ratio

The samples were synthesized under the same gelation temperature, calcination time and calcination temperature conditions but with different M/U molar ratios.

Within the scope of investigation to obtain small-sized ferrite MFe_2O_4 (M=Zn, Co, Ni) single-phase crystals, the optimal M/U molar ratio of 1/2 was selected for the next experiments.

To see more clearly the effect of M/U molar ratio on the morphology, surface properties, and magnetic properties of the sample, we measured IR spectrum, SEM images, N_2 adsorption/desorption isotherms, and magnetic parameters of $NiFe_2O_4$ samples synthesized at three M/U molar ratios: 3/1, 1/1 and 1/2.

The results show that when the M/U molar ratio decreased, the average crystal size decreased from 46 to 34 nm. The specific surface area

of the samples increased from 23.24 to 44.94 m^2/g as the mass of urea in the sample increased. On the FT-IR spectrum of $NiFe_2O_4$ samples, when changing the M/U molar ratio, only a change in the absorption band characteristic of the vibration of the Fe-O bond in the tetrahedral cavities (588 - 596 cm^{-1}) was observed. The mass of urea in the initial synthesized sample also affects the values of magnetic saturation (M_s), remanence (M_r), and coercivity (H_c) of $NiFe_2O_4$ material (Table 3.6). The results show that as the mass of urea in the sample increased, the saturation magnetism value was highest (32.47 $emu.g^{-1}$) with the molar ratio sample M/U=1/2 and reached the lowest value (26, 24 $emu.g^{-1}$) for molar ratio sample M/U=3/1.

3.1.1.4. Effect of pH on the sample synthesis

3.1.2. Some characteristics of ferrite spinels prepared under optimal conditions

Thus, through the investigation process, we have selected the optimal conditions to synthesize pure spinel ferrite samples, as given in Table 3.8.

Table 3.8. Optimal conditions for synthesis of spinel ferrite samples

No.	Ferrite sample	M/U molar ratio	pH	Calcination Temperature (^oC)	Calcination time (h)
1	$ZnFe_2O_4$	1/2	3	500	3
2	$CoFe_2O_4$	1/2	3	500	2
3	$NiFe_2O_4$	1/2	3	500	2

Some characteristics of phase composition and morphology of spinel ferrites prepared under optimal conditions are given in Figures 3.8-3.10.

The XRD pattern confirms the formation of the $ZnFe_2O_4$ spinel crystal structure (PDF 022-1012); $CoFe_2O_4$ (PDF 00-022-1045), and $NiFe_2O_4$ (PDF 00-054-0964).

The EDX spectrum shows the characteristic peaks for elements in the spinel ferrite samples. In addition, other elements can not be detected, proving that the synthesized sample is pure. Scanning and transmission electron microscope images show that the obtained samples are polygonal in shape, with particle sizes ranging from 20 to 60 nm.

The specific surface area of spinel samples synthesized by the combustion method with urea substrate is from 12 m^2/g to 52 $m^{2/}g$ (Table 3.9).

3.1.3. Influence of some factors on the photocatalytic activity of Rhodamine B decomposition of material systems

3.1.3.1. Effect of reaction conditions

To investigate the photocatalytic activity of ferrite to decompose RhB, we conducted experiments under the same conditions of material amount (1.0 g/L), 1.5 mL of 30% H_2O_2, and lighting time of 210 min. The procedure was similar to the process described in section 2.4.2 for the system with spinel ferrite, H_2O_2, and illumination. The dependence of C_t/C_o on the illumination time of the reaction systems is given in Figures 3.11 and 3.12.

Table 3.10. RhB decomposition efficiency of ferrite system in the presence of H_2O_2 and illumination time of 210 min

No.	Reaction system	H(%)
1	H_2O_2 + LED	11.77
2	$ZnFe_2O_4$ + LED	25.35
3	$CoFe_2O_4$ + LED	29.37
4	$NiFe_2O_4$+ LED	10.64
5	$ZnFe_2O_4$ + H_2O_2 + LED	88.05
6	$CoFe_2O_4$ + H_2O_2 + LED	79.57
7	$NiFe_2O_4$+ H_2O_2 + LED	76.77

From Table 3.10, it can be seen that the ferrite system is capable of degrading RhB under research conditions.

3.1.3.2. Effect of metal/urea molar ratio on the RhB degradation photocatalytic activity

We investigated $NiFe_2O_4$ samples at three M/U molar ratios of 1/2, 1/1 and 3/1 for photocatalytic activity in degradation of RhB. With the presence of $NiFe_2O_4$, a decrease in intensity at wavelength 553 nm was observed on the UV-Vis spectrum of RhB solution when increasing the illumination time. After 270 minutes of illumination, the degradation efficiency of RhB increased from 63.75% (with samples with molar ratio M/U=3/1) to 94.66% (with samples with molar ratio M/U= 1/2).

3.1.3.2. Effect of calcination temperature on the RhB degradation photocatalytic activity

We selected four $CoFe_2O_4$ catalyst samples calcined at temperatures from 500 to 800^oC to investigate the photocatalytic activity of RhB decomposition.

The results showed that after 270 minutes of illumination, the RhB degradation efficiency in the presence of H_2O_2 and $CoFe_2O_4$ was 90.6%, 67.6%, 51.6%, and 42.8%, respectively, corresponding to the $CoFe_2O_4$ samples calcined at 500 to 800^oC. Thus, when increasing the calcination temperature of the $CoFe_2O_4$ sample, the RhB degradation efficiency decreased.

3.2. Ferrite system doped with rare earth ions La^{3+} and Nd^{3+}

3.2.1. Some characteristics of ferrite materials doped with La^{3+}, Nd^{3+}

3.2.1.1. XRD pattern

The results show that the $ZnLa_xFe_{2-x}O_4$ samples (x =0 ÷ 0.05) have diffraction peaks at the 2θ angles and corresponding lattice planes: 30.0^o (220), 35.28^o (311), 42.92^o (400), 56.66^o (511), 62.18^o (440), and 70.66^o (533). They are characteristic peaks of the spinel structure of $ZnFe_2O_4$ (PDF 022-1012). The presence of doped La^{3+} (La_2O_3) ion in $ZnLa_xFe_{2-x}O_4$ samples is confirmed by the peaks at 2θ angles: 26.14^o, 31.9^o, 39.2^o, 45.8^o, 52.38^o and 60,3^o, corresponding to the hexagonal structure.

XRD measurement results of $ZnNd_xFe_{2-x}O_4$ samples (x =0÷0.05) show that all the samples are single spinel phases. $ZnFe_2O_4$ samples have crystal sizes that decrease from 22 nm to 12 nm as the amount of Nd^{3+} ions doped in the sample increases (Table 3.14). The $ZnFe_2O_4$ lattice constant increased from 8.44 to 8.45Å as the amount of Nd^{3+} increased.

The XRD patterns of the $CoNd_xFe_{2-x}O_4$ (x=0.0÷0.05) samples show that all the $CoNd_xFe_{2-x}O_4$ (x =0 ÷ 0.05) samples have peaks at 2θ angle and the lattice plane: 30.2^o (220), 35.3^o (311), 43.2^o (400), 54.48^o (422), 57.1^o (511), 62.7^o (400) and 70.7^o (533). They are characteristic peaks of the spinel structure of $CoFe_2O_4$ (PDF 03-0864).

When the amount of doped Nd^{3+} ions increased to 0.05, in the $CoNd_{0,05}Fe_{1,95}O_4$ sample, there was $NdFeO_3$ phase due to the replacement of Fe^{3+} ions with Nd^{3+} ions. However, because the ionic radius of Nd^{3+} is

larger than that of Fe^{3+}, this substitution in the $CoFe_2O_4$ crystal lattice is limited. The intensity of the diffraction peak of the (311) lattice plane increased, and there was a slight shift of the 2θ angle upward (to the smaller 2θ angle), indicating that there was a transfer of Nd^{3+} ions into the tetrahedral and octahedral cavities to replace ions Co^{2+}/Fe^{3+}.

The results (Table 3.15) show that when the amount of doping Nd^{3+} ions increased, the crystal size increased (14.35÷29.14 nm), the volume of the lattice cell and the lattice constant increased. This is explained by the fact that the substitution of Nd^{3+} ions has expanded the lattice cell.

3.2.1.2 FT-IR spectrum

The FT-IR spectra of the samples $ZnLa_xFe_{2-x}O_4$, $ZnNd_xFe_{2-x}O_4$ and $CoNd_xFe_{2-x}O_4$ (x=0÷0.05) are given in Figure 3.19. All the spectra have characteristic vibrations of metal-oxygen bonds (M-O) in the tetrahedral cavity ($\overline{\nu_1}$) and octahedral cavity ($\overline{\nu_2}$) (Table 3.16). The wavenumber values $\overline{\nu_1}$ and $\overline{\nu_2}$ of all the La^{3+} and Nd^{3+} doped ferrite samples changed and were higher than those in the pure sample.

3.2.1.3. Energy-dispersive X-ray (EDX) spectra

EDX spectra and atomic percentages in the samples are given in Figures 3.20-3.21. On the EDX spectra of samples $ZnFe_2O_4$ (Figure 3.20a) and $CoFe_2O_4$ (Figure 3.21a), characteristic peaks of Zn, Co, Fe and O can be observed. The characteristic peaks of La and Nd in the doped $ZnFe_2O_4$ and $CoFe_2O_4$ samples are also detected on the EDX spectra (Figures 3.20 (b,c) and 3.21). Besides, the characteristic peaks of other elements can not be observed, proving that the obtained samples were pure. The percentage of atoms in the samples calculated from EDX data is relatively consistent with the theoretical results (Table 3.17).

3.2.1.4. UV–Vis Diffuse Reflectance Spectrum

The results show that the band gap energy value of the rare earth-doped samples is lower than that of the pure sample. The bandgap energy value of the $CoFe_2O_4$ and $ZnFe_2O_4$ samples decreased as the content of La^{3+} and Nd^{3+} ions increased.

3.2.1.5. Morphology and specific surface area

Scanning electron microscope (SEM) and transmission electron microscope (TEM) images of $ZnFe_2O_4$, $ZnLa_{0,05}Fe_{1,95}O_4$, $ZnNd_xFe_{2-x}O_4$

samples (x=0 ÷ 0.05), $CoFe_2O_4$ and $CoNd_{0,05}Fe_{1,95}O_4$ samples are given in Figure 3.25, 3.26, 3.27, 3.28. The results show that the obtained nanoparticles are polygonal in shape and relatively uniform in size.

The $ZnLa_{0,05}Fe_{1,95}O_4$ sample has a particle size distribution of 40 nm (Figure 3.25f), smaller than that of the pure $ZnFe_2O_4$ sample (60 nm) (Figure 3.25e). The decrease in particle size can be explained by the influence of La^{3+} ions, which prevent the growth of $ZnFe_2O_4$ crystals. There is a slight decrease in average particle size from 35 nm ($CoFe_2O_4$) to 30 nm ($CoNd_{0,05}Fe_{1,95}O_4$) (Figure 3.28).

The N_2 gas adsorption/desorption isotherms and the pore size distribution of the two samples $ZnFe_2O_4$ and $ZnLa_{0,05}Fe_{1,95}O_4$ are given in Figure 3.30. According to Figure 3.30 a,b, the isotherms of both material samples have a combination of types III and IV, typical for mesoporous and macroporous materials according to the IUPAC classification. However, the isotherm of the $ZnLa_{0,05}Fe_{1,95}O_4$ material has a more obvious hysteresis loop width than that of pure $ZnFe_2O_4$. Figures 3.30 c and d show that the pore size of $ZnFe_2O_4$ is 60 nm, and that of $ZnLa_{0,05}Fe_{1,95}O_4$ is 30 nm. This result is also consistent with SEM and TEM data. The $ZnFe_2O_4$ material belongs to the macroporous type (>50 nm), while the $ZnLa_{0,05}Fe_{1,95}O_4$ material belongs to the mesoporous type (2-50 nm). In addition, the measurement results show that the specific surface area of the $ZnLa_{0,05}Fe_{1,95}O_4$ material is 41.07 m^2/g, higher than that of pure $ZnFe_2O_4$ (9.99 m^2/g). The total pore volume of the material $ZnLa_{0,05}Fe_{1,95}O_4$ is higher than that of $ZnFe_2O_4$, while the average pore size of this material is lower than that of $ZnFe_2O_4$ (Table 3.19).

The N_2 adsorption/desorption isotherm and the pore size distribution of the two samples $CoFe_2O_4$ and $CoNd_{0,05}Fe_{1,95}O_4$ are given in Figure 3.31. The results demonstrate that the isotherm of $CoFe_2O_4$ material belongs to type II according to the IUPAC classification, typical for mesoporous material.

In addition, the measurement results determined that the specific surface area of $CoNd_{0.05}Fe_{1.95}O_4$ material is 35.0 m^2/g, higher than that of pure $CoFe_2O_4$ (12.7 m^2/g). The total pore volume of $CoNd_{0.05}Fe_{1.95}O_4$

material is higher than that of $CoFe_2O_4$ while the average pore width of this material is lower than that of $CoFe_2O_4$ (Table 3.19).

Table 3.19. Textual properties of $ZnFe_2O_4$, $ZnLa_{0,05}Fe_{1,95}O_4$, $ZnNd_{0,03}Fe_{1,97}O_4$, $CoFe_2O_4$, $CoNd_{0,05}Fe_{1,95}O_4$ nanoparticles

Surface property	Specific surface area (m^2/g)	Total pore volume (cm^3/g)	Average pore width (nm)
$ZnFe_2O_4$	9,99	0,087	38,48
$ZnLa_{0,05}Fe_{1,95}O_4$	41,07	0,186	22,34
$ZnNd_{0,03}Fe_{1,97}O_4$	28,86	0,21	28,00
$CoFe_2O_4$	12,7	0,099	32,8
$CoNd_{0,05}Fe_{1,95}O_4$	35,0	0,114	12,6

3.2.1.6. Magnetic properties

The hysteresis curves of the samples are given in Figure 3.32

Table 3.20. Magnetic parameter of $CoNd_xFe_{2-x}O_4$ (x = 0÷0,05) nanoparticles

STT	Sample	Magnetic saturation (emu/g)	Remanence (emu/g)	Coercivity (Oe)
1	$CoFe_2O_4$	47,78	21,5	1972,22
2	$CoNd_{0,01}Fe_{1,99}O_4$	43,97	17,38	1766,94
3	$CoNd_{0,03}Fe_{1,97}O_4$	41,69	15,8	1317,26
4	$CoNd_{0,05}Fe_{1,95}O_4$	28,99	10,45	1199,95

The results show that as the amount of Nd^{3+} ions in the sample increased, the magnetic saturation, remanence, and coercivity decreased (Table 3.20). When doped with Nd^{3+} ions, the magnetic properties of $CoFe_2O_4$ material change.

3.2.2. Photocatalytic activity in RhB degradation of ferrite materials doped with La^{3+}, Nd^{3+}

3.2.2.1. Effect of rare-earth ions

UV-Vis spectra of RhB solution after time intervals of illumination in the simultaneous presence of H_2O_2 and the materials $ZnLa_xFe_{2-x}O_4$, $ZnNd_xFe_{2-x}O_4$ and $CoNd_xFe_{2-x}O_4$ (x = 0 ÷ 0.05) are presented in Figures

3.33 - 3.35. The results show that $ZnFe_2O_4$ samples doped with Nd^{3+} ions have a higher RhB degradation efficiency than that of pure $ZnFe_2O_4$ samples. The reason is that the crystalline size of the $ZnNd_xFe_{2-x}O_4$ samples (x = 0.0 ÷ 0.05) decreased from 22 nm to 12 nm as the amount of Nd^{3+} in the sample increased. On the other hand, the band gap energy of the $ZnNd_xFe_{2-x}O_4$ samples (x =0.0 ÷ 0.05) decreased from 1.75 eV to 1.42 eV when the amount of Nd^{3+} increased, which also contributes to enhancing the formation of radicals $^{\bullet}OH$ and stimulating the breakdown of RhB molecules.

When doped with rare earth ions La^{3+}, Nd^{3+}, the RhB degradation efficiency of ferrites increases significantly (Table 3.21). The reason is that the presence of La^{3+} and Nd^{3+} ions in the sample reduces the recombination of electrons and holes. Therefore, the photocatalytic activity of the materials samples is enhanced. For $ZnFe_2O_4$ doped with La^{3+}, it increased from 73.04% to 86.3%; for $ZnFe_2O_4$ doped with Nd^{3+}, it increased from 85,14% to 95.46%; and for $CoFe_2O_4$ doped with Nd^{3+}, it increased from 71.7% to 94.7%.

To determine the kinetics of the RhB degradation reaction, we calculate the $\ln(C/C_o)$ values versus time. The results show that the RhB degradation reaction on the catalyst $ZnLa_xFe_{2-x}O_4$, $ZnNd_xFe_{2-x}O_4$ and $CoNd_xFe_{2-x}O_4$ (x=0 ÷ 0.05) obeys the first-order kinetic equation. When La^{3+} and Nd^{3+} ions are present in the $ZnFe_2O_4$ and $CoFe_2O_4$ crystals, the reaction rate constant of RhB degradation reaction decreases (Table 3.21d).

3.2.2.2. Effect of H_2O_2 concentration

The calculation results show that when the concentration of H_2O_2 increased from 0.05 M to 0.1 M, the RhB degradation efficiency increased from 79.38% to 97.42% for % $ZnLa_{0,05}Fe_{1,95}O_4$, from 79.4% to 97.2% for $ZnNd_{0,03}Fe_{1,97}O_4$ and from 81.04% to 93.52% for $CoNd_{0,05}Fe_{1,95}O_4$. However, when the concentration of H_2O_2 increased to 0.15M, the efficiency decreased. The optimal concentration of H_2O_2 for RhB degradation, when illuminated with the presence of $ZnLa_{0,05}Fe_{1,95}O_4$, $CoNd_{0,05}Fe_{1,95}O_4$ and $ZnNd_{0,03}Fe_{1,97}O_4$ materials, is 0.1 M.

3.2.2.3. Effect of material dose

Figure 3.40 shows that when the dose of the material increased from 0.5 to 0.75 g/L, the RhB degradation efficiency increased from 62.13% to 98.01% for $ZnLa_{0,05}Fe_{1,95}O_4$, from 62. 13% to 98.01% for $ZnNd_{0,03}Fe_{1,97}O_4$ and from 72.52% to 93.52% for $CoNd_{0,05}Fe_{1,95}O_4$. When the dose of the material increased to 1.0 g/L, the decomposition efficiency decreased to 93.03% for $ZnLa_{0,05}Fe_{1,95}O_4$, 93.02% for $ZnNd_{0,03}Fe_{1,97}O_4$, and 88.14% for $CoNd_{0,05}Fe_{1,97}O_4$. The optimal dose of $ZnLa_{0,05}Fe_{1,95}O_4$, $ZnNd_{0,03}Fe_{1,97}O_4$ and $CoNd_{0,05}Fe_{1,97}O_4$ for RhB degradation is 0.75 g/L.

3.2.3. Effect of inhibitors

To evaluate the role of free radicals $^{\bullet}O_2^-$, $^{\bullet}OH$ and holes (h^+) in the photocatalytic reaction of RhB degradation of the $ZnLa_{0,05}Fe_{1,95}O_4/H_2O_2$/Led system and the $CoNd_{0,05}Fe_{1,95}O_4/H_2O_2$/Led system, the experiments were carried out in the absence and presence of inhibitors such as ascorbic acid ($^{\bullet}O_2^-$inhibitor), isopropyl alcohol (IPA) ($^{\bullet}OH$ inhibitor) and ethylenediaminetetraacetic acid (EDTA) (h^+ inhibitor). The results show that the RhB degradation efficiency and reaction rate constant of the $ZnLa_{0,05}Fe_{1,95}O_4/H_2O_2$/Led system and the $CoNd_{0,05}Fe_{1,95}O_4/H_2O_2$/Led decreased in the presence of ascorbic acid, EDTA and IPA(Table 3.22-3.23). The $ZnLa_{0,05}Fe_{1,95}O_4/H_2O_2$/Led system had the highest reduction in RhB degradation efficiency (from 99.5% to 38.87%) in the presence of IPA. From this result, it can be assumed that the $^{\bullet}OH$ radicals play the primary role in the RhB degradation process of the $ZnLa_{0,05}Fe_{1,95}O_4/H_2O_2$/Led system. However, for the $CoNd_{0,05}Fe_{1,95}O_4/H_2O_2$/Led system, the decrease in RhB degradation efficiency in the presence of ascorbic acid, EDTA, and IPA is not significantly different. Thus, $^{\bullet}OH$, $^{\bullet}O_2^-$, and h^+ are essential for the RhB degradation process of the $CoNd_{0,05}Fe_{1,95}O_4/H_2O_2$/Led system.

According to the results, we propose the RhB degradation reaction mechanism on $ZnFe_2O_4$ catalysts doped with La^{3+} ions and $CoFe_2O_4$ doped with Nd^{3+} ions as follows: when properly illuminated, a photocatalytic process occurs on the surface of $ZnLa_xFe_{2-x}O_4$ and $CoNd_xFe_{2-x}O_4$, creating free radicals with high oxidation potential such as $^{\bullet}OH$, $^{\bullet}O_2^-$, which degrade organic compounds as the following:

$$ZnLa_xFe_{2-x}O_4 + h\nu \rightarrow e^- + h^+$$

$$CoNd_xFe_{2-x}O_4 + h\nu \rightarrow e^- + h^+$$

$$e^- + O_2 \rightarrow {}^{\bullet}O_2^-$$

$$H_2O_2 + e^- \rightarrow {}^{\bullet}OH + OH^-$$

$$h^+ + H_2O \rightarrow {}^{\bullet}OH + H^+$$

$$h^+ + OH^- \rightarrow {}^{\bullet}OH$$

$${}^{\bullet}OH/{}^{\bullet}O_2^- + RhB \rightarrow CO_2 + H_2O + \ldots.$$

$$\equiv Fe^{3+} + e^- \rightarrow \equiv Fe^{2+}$$

$$\equiv Fe^{3+} + H_2O_2 \rightarrow \equiv Fe^{2+} + {}^{\bullet}OOH + H^+$$

$$\equiv Fe^{2+} + H_2O_2 \rightarrow \equiv Fe^{3+} + {}^{\bullet}OH + OH^-$$

$$RhB + ({}^{\bullet}OH, {}^{\bullet}O_2^-, {}^{\bullet}OOH) \rightarrow CO_2, H_2O$$

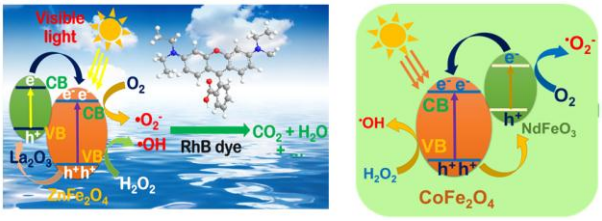

Figure 3.43. Illustration of the photocatalytic reaction mechanism of RhB degradation by $ZnLa_xFe_2$-xO_4 and $CoNd_xFe_{2-x}O_4$ materials in the presence of light and H_2O_2

3.2.4. The ability to recover and reuse materials

The RhB degradation efficiency after three cycles of La^{3+} and Nd^{3+} doped ferrite materials is given in Figure 3.44.

After three cycles, the RhB degradation efficiency of $ZnLa_{0,05}Fe_{1,95}O_4$ material decreased from 98.01% to 70.0%; that of $ZnNd_{0,05}Fe_{1,95}O_4$ decreased from 96.0% to 72.02%, and that of $CoNd_{0,05}Fe_{1,95}O_4$ decreased from 94.03% to 78.01%.

The surface and phase composition of the $ZnLa_{0,05}Fe_{1,95}O_4$ material are almost unchanged (Figure 3.45-3.46). This proves that the materials are highly durable and can be applied to treat organic compounds in wastewater.

3.2.5. Testing textile wastewater treatment of material samples

The change in COD value of textile wastewater versus the lighting time in the presence of material samples $ZnLa_xFe_{2-x}O_4$ and $CoNd_xFe_{2-x}O_4$ (x =0 ÷0.05) is given in Figures 3.47 and 3.48. It can be seen that when the lighting time increased, the COD value of textile wastewater decreased.

Among the material samples, $ZnLa_{0,05}Fe_{1,95}O_4$ and $CoNd_{0,05}Fe_{1,95}O_4$ had the highest reduciton in COD values. After 360 min of illumination in the presence of H_2O_2, the COD index of the $ZnLa_{0,05}Fe_{1,95}O_4$ system decreased by 88.67% (from 364.67 mg/L to 41.33 mg/L), that of the $CoNd_{0,05}Fe_{1,95}O_4$ system decreased by 89.61% (from 394.7 mg/L to 41.0 mg/L).

3.3. Characteristics of structure and RhB photocatalytic degradation activity of $ZnFe_2O_4$/Bentonite composite system

3.3.1. Characteristics of the $ZnFe_2O_4$/Bentonite materials

The XRD patterns of bentonite, $ZnFe_2O_4$, and $ZnFe_2O_4$/BT are shown in Figure 3.49. From Figure 3.49 (a), it can be seen a peak at 2θ of 26.37^o (003) which is typical for bentonite (PDF 03-0019). The peaks observed at 2θ angles of 30.08^o (220); 35.48^o (311); 43.16^o (400); 57.0^o (511) and 62.6^o (440) (Figure 3.49(a)) are characteristic peaks for the cubic structure of $ZnFe_2O_4$ (PDF 022-1012).

The characteristic peaks of $ZnFe_2O_4$ are observed on the XRD pattern of the $ZnFe_2O_4$/BT sample (Figure 3.49a(3). However, their intensity is lower than that of the pure $ZnFe_2O_4$ sample. The decrease in the intensity of the peaks proved an interaction between $ZnFe_2O_4$ and bentonite. Calculation results from the Deby-Scherrer equation show that the crystallite size of $ZnFe_2O_4$/BT is 22 nm, smaller than that of pure $ZnFe_2O_4$ (29 nm).

The FT-IR spectrum of bentonite shows absorption bands at 3693-3620 and 690 cm^{-1}, characterizing the vibrations of Al-(OH) and Si-O bonds. The absorption bands at 3394 and 1633 cm^{-1} are due to the vibrations of the O-H bond in the water molecule present on the bentonite surface. The absorption bands at 910 and 794 cm^{-1} confirmed the presence of diocta groups and SiO_2 in bentonite. The absorption band at 991 cm^{-1} is attributed to the vibration of the Si-O bond. From Figure 3.49b (2), it can be seen that there is a strong absorption band at 522 cm^{-1} that is due to the vibration of the Zn-O bond in the tetrahedral cavity and a band at 447 cm^{-1}, relating to the Fe-O bond in the octahedral cavities of $ZnFe_2O_4$. The FT-IR spectrum of $ZnFe_2O_4$/BT shows a change in the vibrations of the metal-oxygen (M-O) bond in both tetrahedral and octahedral cavities. This proves that the MMT layers in bentonite have affected the vibrations of the M-O bonds. In addition, there are additional

absorption bands at 773 cm-1 and 1037 cm^{-1} that can be contributed to the vibrations of the SiO_2 group and the Si-O-Si bond. The change in the absorption band of these two groups demonstrates the formation of $ZnFe_2O_4$/BT composite. The absorption band at 3379 cm^{-1} characterizing the vibration of the O-H bond in the water molecule present on the surface of the $ZnFe_2O_4$/BT sample was also observed.

SEM images of $ZnFe_2O_4$ and $ZnFe_2O_4$/BT samples (Figure 3.51) show that the obtained particles have a polygonal shape and uniform distribution. There was an obvious decrease in agglomeration in the $ZnFe_2O_4$/BT sample. The particle size of the $ZnFe_2O_4$/BT sample (about 30 nm) is smaller than that of the $ZnFe_2O_4$ sample (about 45-50 nm).

The calculation shows that the band gap energy of the $ZnFe_2O_4$/BT sample is 1.82 eV, smaller than those of bentonite (2.18 eV) and $ZnFe_2O_4$ (1.95 eV).

Both $ZnFe_2O_4$ and $ZnFe_2O_4$/BT samples have isotherms of type IV according to the IUPAC classification, typical for mesoporous materials. The specific surface area of the $ZnFe_2O_4$/BT sample (23.79 m^2/g) is larger than that of $ZnFe_2O_4$ (16.11 m^2/g). The total pore volume and average pore diameter of the $ZnFe_2O_4$/BT sample are 0.1450 cm^3/g and 27.45 nm, respectively, smaller than those of the pure $ZnFe_2O_4$ sample (0.1457 cm^3/g; 38.70 nm). With the increase in specific surface area and decrease in volume and pore diameter, the $ZnFe_2O_4$/BT sample promises to have better adsorption capacity than the pure $ZnFe_2O_4$ sample.

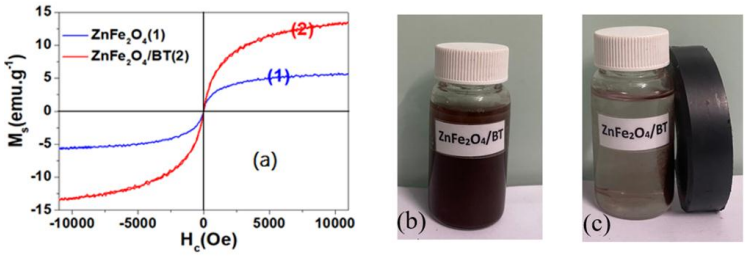

Figure 3.54. Hysteresis curves (a) of samples $ZnFe_2O_4$ (1), $ZnFe_2O_4$/BT(2), and the mixture containing $ZnFe_2O_4$/BT at the beginning (b) and after placing the magnet for 15 minutes (c)

The results show that the magnetic saturation value (M_s) of the $ZnFe_2O_4$/BT sample is 13.42 emu/g, higher than that of the $ZnFe_2O_4$ sample (5.61 emu/g). When mixed with bentonite, there is a decrease in

particle size and a rearrangement of the spin magnetic moment in $ZnFe_2O_4$. Therefore, it increases the magnetic saturation of the $ZnFe_2O_4$/BT material. Hence, the $ZnFe_2O_4$/BT material can be easily separated from the solution after the reaction using a magnet.

3.3.2. RhB photocatalytic degradation activity of $ZnFe_2O_4$/Bentonite material

The RhB adsorption and degradation ability of the samples was studied under conditions of without light and with LED light for 210 minutes. RhB degradation efficiency of H_2O_2 only reached 10.02% without light (Figure 3.55a(1)) and increased slightly with LED light (11.77%) (Figure 3.55b(1)) after 210 minutes of reaction. When the system contains only $ZnFe_2O_4$ and without light, the RhB adsorption efficiency reached 13.2% (Figure 3.55a(2)) and increased slightly to 17.59% with LED light (Figure 3.55b(2)).

For the system containing $ZnFe_2O_4$ and H_2O_2 without light, only 29.13% of the RhB molecules can be decomposed (Figure 3.55a(3)), but when the LED light was applied, the RhB treatment efficiency increased sharply, reaching 88.05% (Figure 3.55b(3)). When only the $ZnFe_2O_4$/BT was present for 210 minutes, the RhB adsorption efficiency of the material reached 30.34% (without light, Figure 3.55a(4)) and 39.80% (with light, Figure 3.55b(4)). When the oxidant H_2O_2 was added to this system without lighting, the treatment efficiency only reached 40.92% (Figure 3.55a(5)). With the presence of LED light, the RhB treatment efficiency of this system increased to 93.23% (Figure 3.55b(5)).

During this process, free radicals are continuously generated, so the organic compound decomposition efficiency of the ferrite/H_2O_2/LED system is improved. When $ZnFe_2O_4$ was hosted on the bentonite substrate, the RhB degradation performance of this material was significantly enhanced.

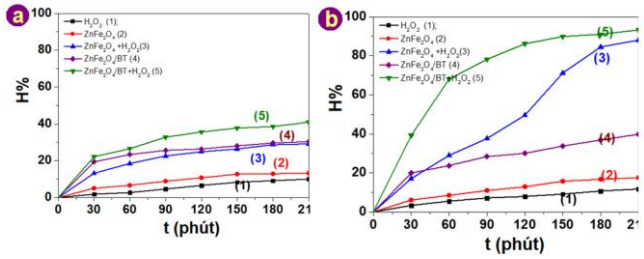

Figure 3.55. Dependence of the RhB degradation efficiency (%H) on time of the system without light (a) and with light (b) in the presence of H_2O_2 (1), $ZnFe_2O_4$ (2), $ZnFe_2O_4$+H_2O_2 (3), $ZnFe_2O_4$/BT (4) and $ZnFe_2O_4$/BT+ H_2O_2 (5)

3.3.3. Effect of inhibitors

The results of the effects of free radicals $^{\bullet}O_2^-$, $^{\bullet}OH$, and h^+ in the $ZnFe_2O_4/H_2O_2$/LED and $ZnFe_2O_4$/BT/H_2O_2/LED systems are given in Figure 3.56. Figure 3.56a shows that the RhB degradation efficiency of the $ZnFe_2O_4/H_2O_2$/LED system decreased from 85.15% to 54.09% (ascorbic acid), 62.08% (EDTA) and 38.71% (IPA). The RhB degradation efficiency of the $ZnFe_2O_4$/BT/H_2O_2/LED system (Figure 3.56b) also decreased sharply in the following order: without inhibitor (92.23%) > with EDTA (68.9%) > with ascorbic acid (58.49%)> with IPA (42.96%). This shows that free radicals $^{\bullet}O_2^-$, $^{\bullet}OH$ and h^+ play an important role in the photocatalytic process of $ZnFe_2O_4/H_2O_2$/LED and $ZnFe_2O_4$/BT/H_2O_2/LED systems. The effect of free radicals on the degradation efficiency of organic compounds has been shown in the previous studies on the material systems $MnFe_2O_4$/Bentonite and $NiFe_2O_4$/Bentonite, $ZnFe_2O_4$/Bentonite.

Based on the above research results, a diagram of the RhB photocatalytic degradation mechanism of the $ZnFe_2O_4$/BT/H_2O_2/LED system can be depicted in Figure 3.57.

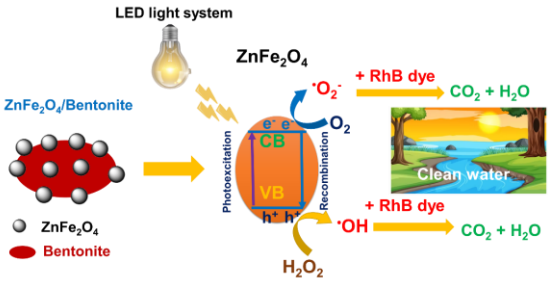

Figure 3.57. Diagram presenting the RhB photocatalytic degradation mechanism of $ZnFe_2O_4$/BT/H_2O_2/LED system

$ZnFe_2O_4$/BT material is an effective catalyst in decomposing organic pollutants such as RhB under visible light.

3.3.4. The ability to recover and reuse materials

After three times of use, the RhB degradation efficiency of $ZnFe_2O_4$/BT material decreased from 93.23% to 75.0%. The surface and phase composition of $ZnFe_2O_4$/BT material remains almost unchanged (Figure 3.59). This proves that the materials have high durability and have the ability to be applied in practice to treat polluted organic compounds.

3.3.5. Testing textile wastewater treatment of $ZnFe_2O_4$/BT material

The results show that the $ZnFe_2O_4$/BT material sample could reduce the COD value strongly. After 360 minutes of illumination in the presence of H_2O_2, the COD index of the $ZnFe_2O_4$/BT system decreased by 91.19% (from 431.33 mg/L to 38 mg/L. The majority of RhB molecules with aromatic rings are decomposed into smaller molecules. This is followed by the complete mineralization of RhB into less toxic substances.

CONCLUSION

1. According to the research results of some factors affecting the phase formation and crystal size of the spinel ferrite MFe_2O_4 (M=Zn, Co, Ni) system, including calcination temperature, M/urea molar ratio, calcination time, and pH, the appropriate conditions to synthesize single-phase spinel systems of ferrite MFe_2O_4 (M=Zn, Co, Ni), with small crystallite size are calcination temperature of 500^oC, molar ratio of 1/2, pH of 3, and calcination time of 3 h (for $ZnFe_2O_4$) and 2 h (for $CoFe_2O_4$ and $NiFe_2O_4$).

2. Three ferrite systems ($ZnFe_2O_4$, $CoFe_2O_4$, $NiFe_2O_4$) and 09 samples of these systems doped with La^{3+}, Nd^{3+}ions (1, 3, and 5 %) have been successfully synthesized. The characteristics of phase composition, morphology, specific surface area, and band gap energy of the synthesized material systems have been studied.

3. The RhB photocatalytic degradation activity of the synthesized material systems has been studied. The effect of some factors, such as calcination temperature, M/U molar ratio, material mass, and H_2O_2 on photocatalytic performance was investigated. After 270 minutes of illumination, the RhB degradation efficiency of the $NiFe_2O_4$ increased to

63.75% (for samples with molar ratio M/U=3/1) and 94.66% (for samples with molar ratio M/U= 1/2). For the $CoFe_2O_4$ sample prepared at 500^oC, the RhB degradation efficiency and $CoFe_2O_4$ reached the highest value of 90.6% after 270 minutes of illumination in the presence of H_2O_2.

When doped with rare earth ions La^{3+}, Nd^{3+}, the RhB degradation efficiency of ferrites increased. Namely, the RhB degradation efficiency of $ZnFe_2O_4$ doped with La^{3+} increased from 73.04% to 86.3% after 240 minutes; that of $ZnFe_2O_4$ doped with Nd^{3+} increased to 95.46% after 210 min; and that of $CoFe_2O_4$ doped with Nd^{3+} increased from 71.7% to 94.7% after 180 minutes.

4. Initially, the mechanism of the photocatalytic degradation reaction has been proposed. The results show that the $^{\bullet}OH$ radicals play a major role in the RhB degradation process of the $ZnLa_{0,05}Fe_{1,95}O_4$ system. For the $CoNd_{0,05}Fe_{1,95}O_4$ system, $^{\bullet}OH$, $^{\bullet}O_2^-$ and h^+ are the major role.

After four times of use, the photocatalytic efficiency of the material still reached over 70%. After three times of use, the RhB degradation efficiency decreased from 98.01% to 70.0% (for $ZnLa_{0,05}Fe_{1,95}O_4$); from 96.0% to 72.02%, (for $ZnNd_{0,05}Fe_{1,95}O_4$); from 94.03% to 78.01%, (for $CoNd_{0,05}Fe_{1,95}O_4$); and from 93.23% to 75, 0% (for $ZnFe_2O_4$/BT).

5. Initial testing treatment of textile and dyeing wastewater of sedge mat weaving village in Thai Binh province using material samples $ZnLa_{0,05}Fe_{1,95}O_4$ and $CoNd_{0,05}Fe_{1,95}O_4$. After 360 minutes of illumination in the presence of H_2O_2 shows that the COD index of the $ZnLa_{0,05}Fe_{1,95}O_4$ system decreased by 88.67% (from 364.67 mg/L to 41.33 mg/L), that of the $CoNd_{0,05}Fe_{1,95}O_4$ system decreased by 89.61% (from 394.7 mg/L to 41.0 mg/L), của $ZnFe_2O_4$/BT từ 431,33 mg/L đến 38 mg/L), of $ZnFe_2O_4$/BT decreased by 91.19 % (from 431.33 mg/L to 38 mg/L).